

SPECinc



Diffraction Limited Size and DOF Estimates

Abstract

In this manuscript we describe the process by which we use laboratory measurements together with diffraction theory to improve estimates of depth of field and of the size of particles imaged by the CPI. This has allowed substantial improvements in the particle size distributions derived from the CPI.

Introduction

Due to diffraction* the images of particles taken by the CPI appear out of focus and over sized when the particle is not in the optical systems object plane. These effects are greater the greater the distance from the object plane and the smaller the particle. Also the depth of field (DOF) and thus sample volume varies with particle size. In the laboratory, we took images of spheres at various distances from the object plane. These are used, in effect, to calibrate an algorithm that finds each particle's size and depth of field from the image. The algorithm is based on diffraction theory. This manuscript's outline is as follows. We first describe the laboratory data, then the algorithm, and then present a comparison of real data processed by this algorithm with data from other particle sizing instruments.

Laboratory Particle Images

* Some of these effects can also be caused by the optical system even under the geometrical optics approximation. Here we are assuming these effects are secondary to the diffraction effects. Further laboratory studies will confirm or refute this assumption.

32 (2.2) micron beads

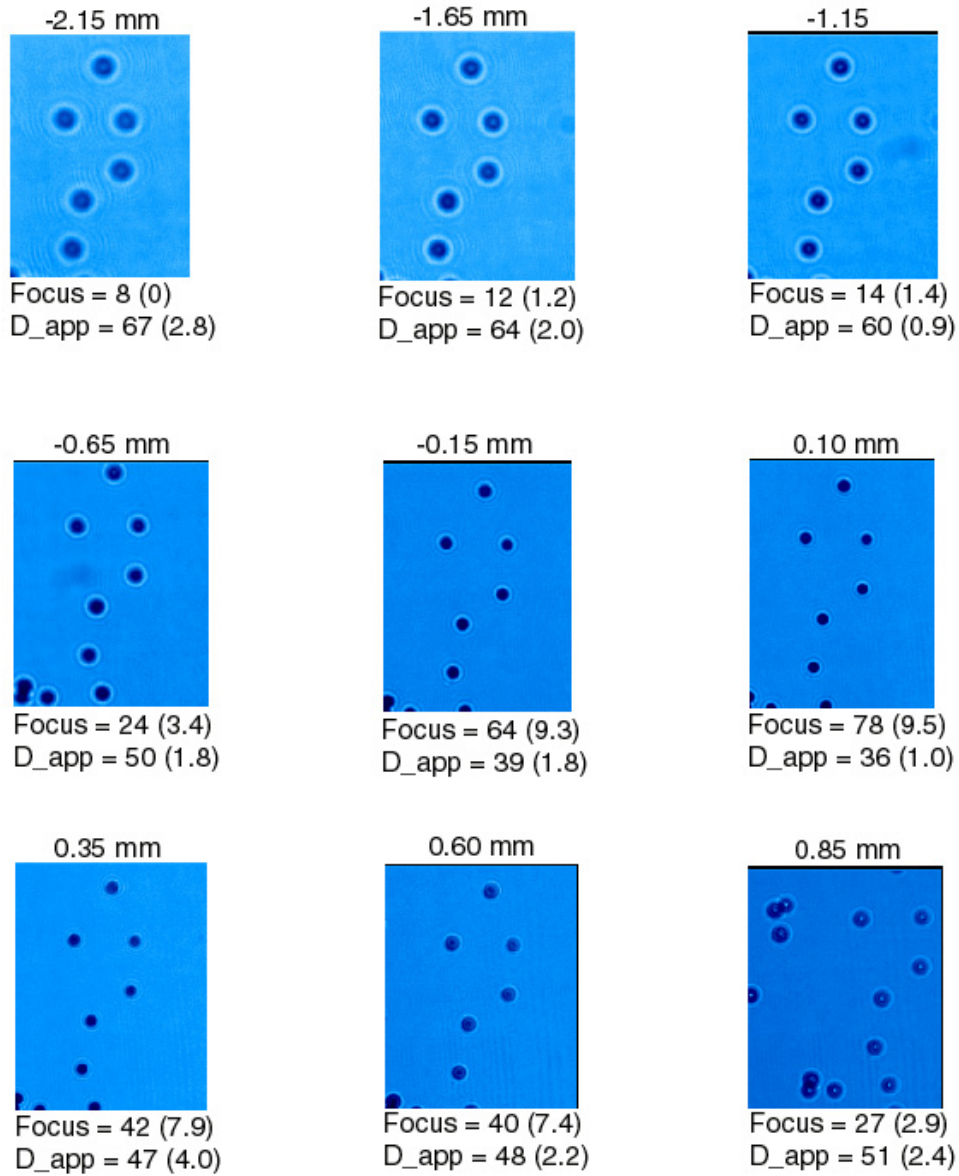
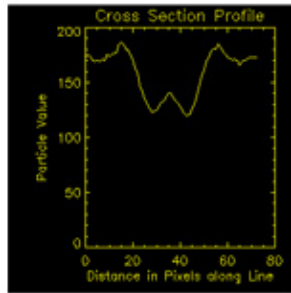
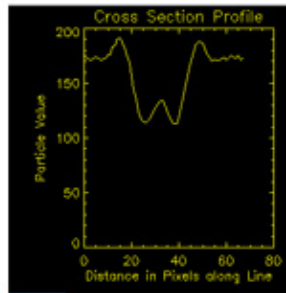


Figure 1: Images of glass beads taken by the CPI in the laboratory at various positions in the sample tube. Above each image box is the distance along the sample tube from the object plane in millimeters. These numbers must be multiplied by $\cos(\pi/2)$ to obtain actual translation along the imaging laser beam direction. Below each image box are the derived focus and size parameters. Standard deviations are in parenthesis.

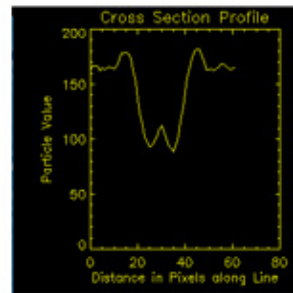
32 micron beads



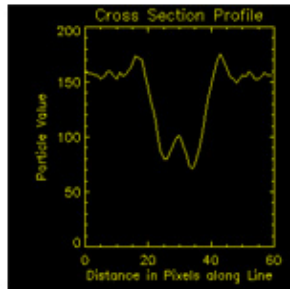
-2.15 mm



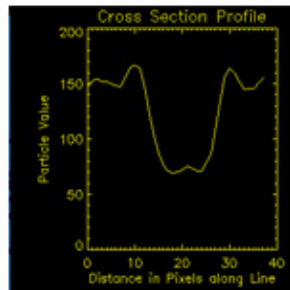
-1.65 mm



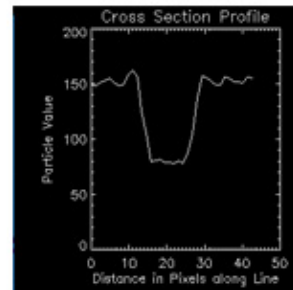
-1.15 mm



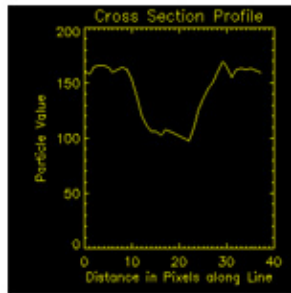
-0.65 mm



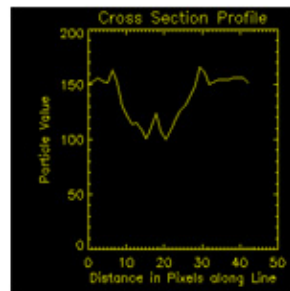
-0.15 mm



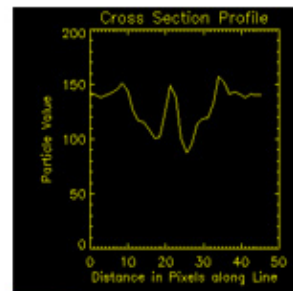
0.10 mm



0.35 mm



0.60 mm



0.85 mm

Figure 2: Intensity cross-sections across the images of the same bead for each position shown in figure 1. Notice the Poisson spots and diffraction rings especially for the more out of focus positions.

Glass beads of diameter $32\ \mu\text{m}$ were placed on a glass slide and moved through the CPI's sample tube with the slide held perpendicular to the imaging laser beam while images were being taken. The slide was moved by means of a micrometer that also gave its position. Examples of images, of the same beads, as their position was varied are shown in figure 1. Our CPI post-processing software was used to determine apparent diameters (D_{app}) and focus values. These were averaged together for four of the particles shown in figure 1. D_{app} is determined by an intensity threshold while focus is determined from the gradient in intensity at the particle's edge. Focus values are normalized so that they equal 100 for a very in focus particle. Examples of the intensity along a line across an image for each image box shown in figure 1 is presented in figure 2. It is evident from these cross-sections as well as from the images that the focus (gradient in intensity) decreases and the apparent size increases the further from the object plane the beads are.

The Algorithm

Let D be the particle diameter, P its distance from the object plane, and λ be the imaging laser's wavelength. The functions $\frac{D_{app}}{D} \left(\frac{P\lambda}{D^2} \right)$ and $focus \left(\frac{P\lambda}{D^2} \right)$ are universal^{*^}. We use the data obtained in the laboratory to determine those universal functions (see figures 3 and 4). For any given image, the measured value of focus and the second function are used to determine its normalized position $\left(\frac{P\lambda}{D^2} \right)$. From the normalized position, its measured D_{app} , and the first function we obtain its actual diameter D . From D and its normalized position we obtain P . Finally we compare its P with a pre-determined DOF for its D and find out if it is acceptable as in depth of field or not. Thus on a particle by particle basis, we find its size and its sample volume.

^{*} Korolev, A. V., J. W. Strapp, and G. A. Isaac. 1998: *J. Atmos. and Oceanic Technol.*, **15**, 708-720.

[^] The results of Korolev et al. are strictly applicable for coherent light. The CPI uses partially coherent light.

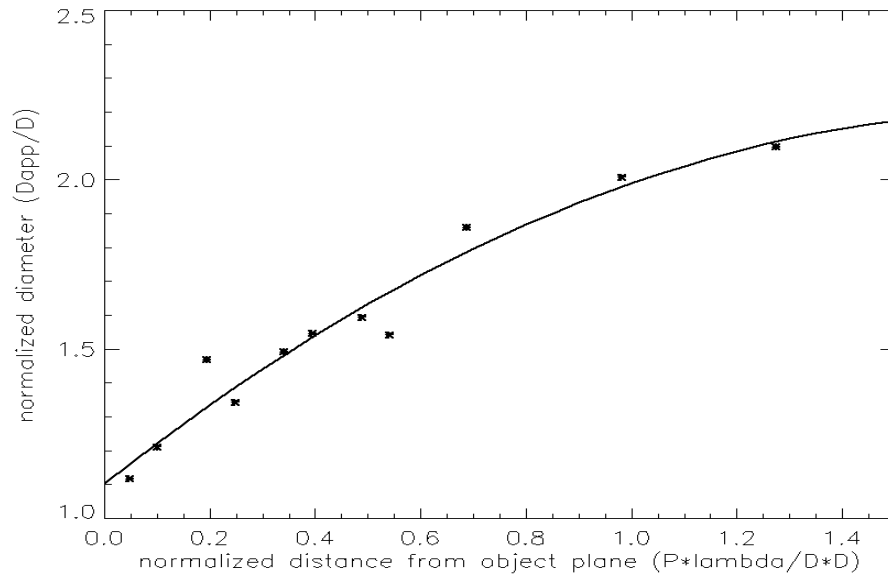


Figure 3: The symbols are data points from the laboratory. The line is the function we fit to the data that is used in the algorithm for estimating size and DOF.

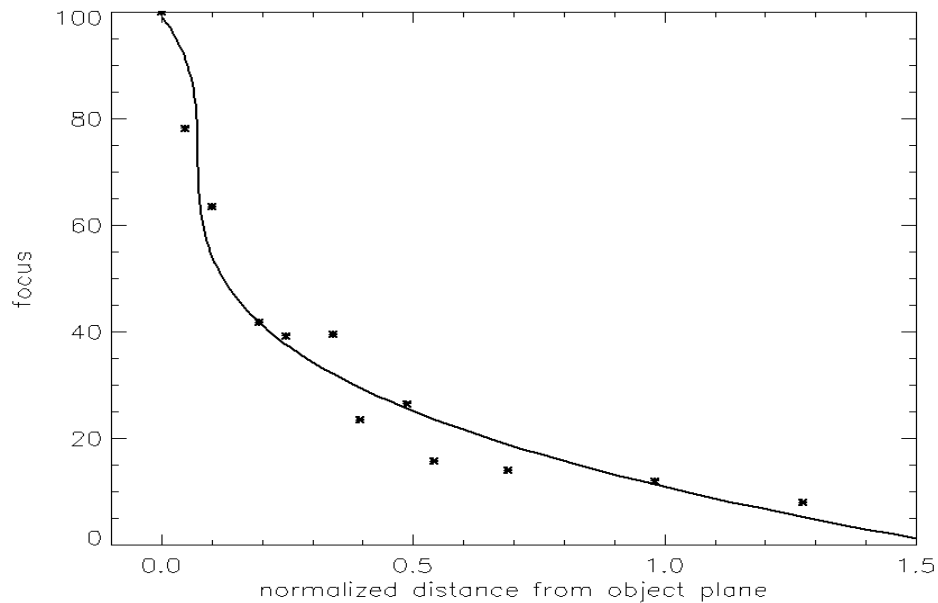


Figure 4: The symbols are data points from the laboratory. The line is the function we fit to the data that is used in the algorithm for estimating size and DOF.

Real Particle Data

The particle size distributions obtained from D and the derived sample volume are significantly improved over those derived from D_{app} and a fixed sample volume. Figure 5 demonstrates the difference while figures 6 through 9 compare the derived particle size distribution with those measured by other instruments. The comparison in figure 6 between real CPI data and FSSP data is made using data collected during the combined FIRE-ACE and SHEBA project. The spectra were averaged over 200 seconds to eliminate any sampling statistics problems. The cloud was a continuous super-cooled liquid-water boundary-layer cloud. Using D instead of D_{app} brings the shape of the CPI size distribution in close agreement with the FSSP size distribution. The sizing difficulties are greatest for these small particles at the small end of the CPI size range. The effect of using the measured DOF instead of the fixed distance between the CPI windows is, as expected, very large for the small particles. The CPI size distribution concentrations are too high. They are about 7 times higher than the FSSP. The FSSP is not likely under-counting as its LWC is already too high[♦].

Figures 7, 8 and 9 show data taken at NASA's icing research wind tunnel. The CPI size distribution is compared with the size distribution measured with NASA's PMS 1D optical array probes and FSSP. Three wind tunnel conditions are shown. The CPI size distributions based on the focus estimated sizes and DOFs are much better than the raw data. The concentration estimates again tend to be too high at the small end of the size range, especially for the case with the largest drops, where the cloud was most inhomogeneous.

[♦] Lawson, R.P., B.A. Baker, C.G. Schmitt and T. L. Jensen 2001: An overview of microphysical properties of Arctic stratus clouds observed during FIRE.ACE. *J. Geophys. Res.* **106** d14.

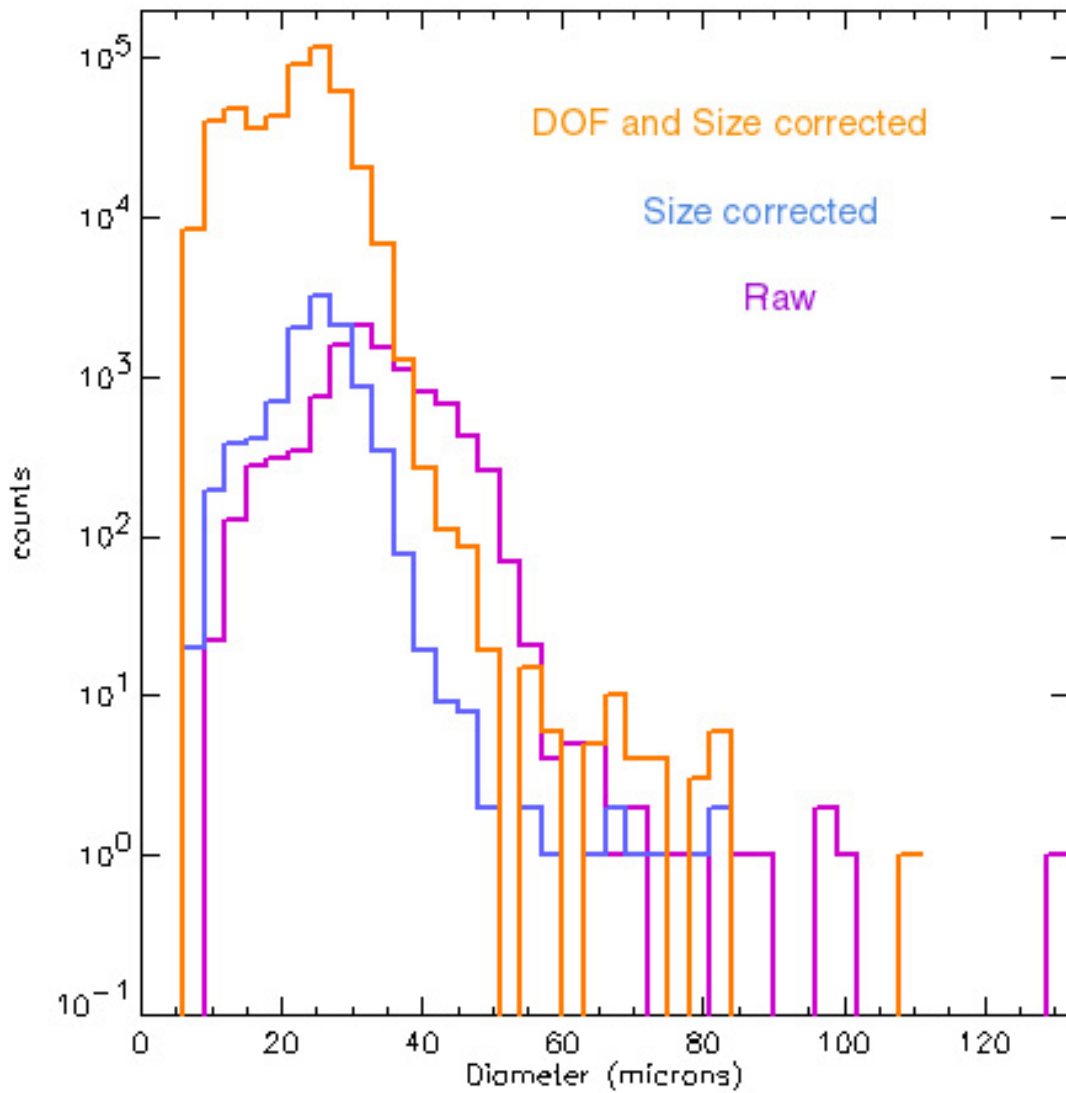


Figure 5: The violet distribution is of D_{app} in raw counts per bin. The blue distribution is of D in raw counts per bin. The orange distribution is of D with the counts per bin inflated according to the sample volume for that size. That is, The counts per bin (of the blue distribution) has been multiplied by DOF_{max}/DOF to create the orange distribution. DOF_{max} is the distance between the windows of the CPI and DOF is the predetermined value for that bin's size.

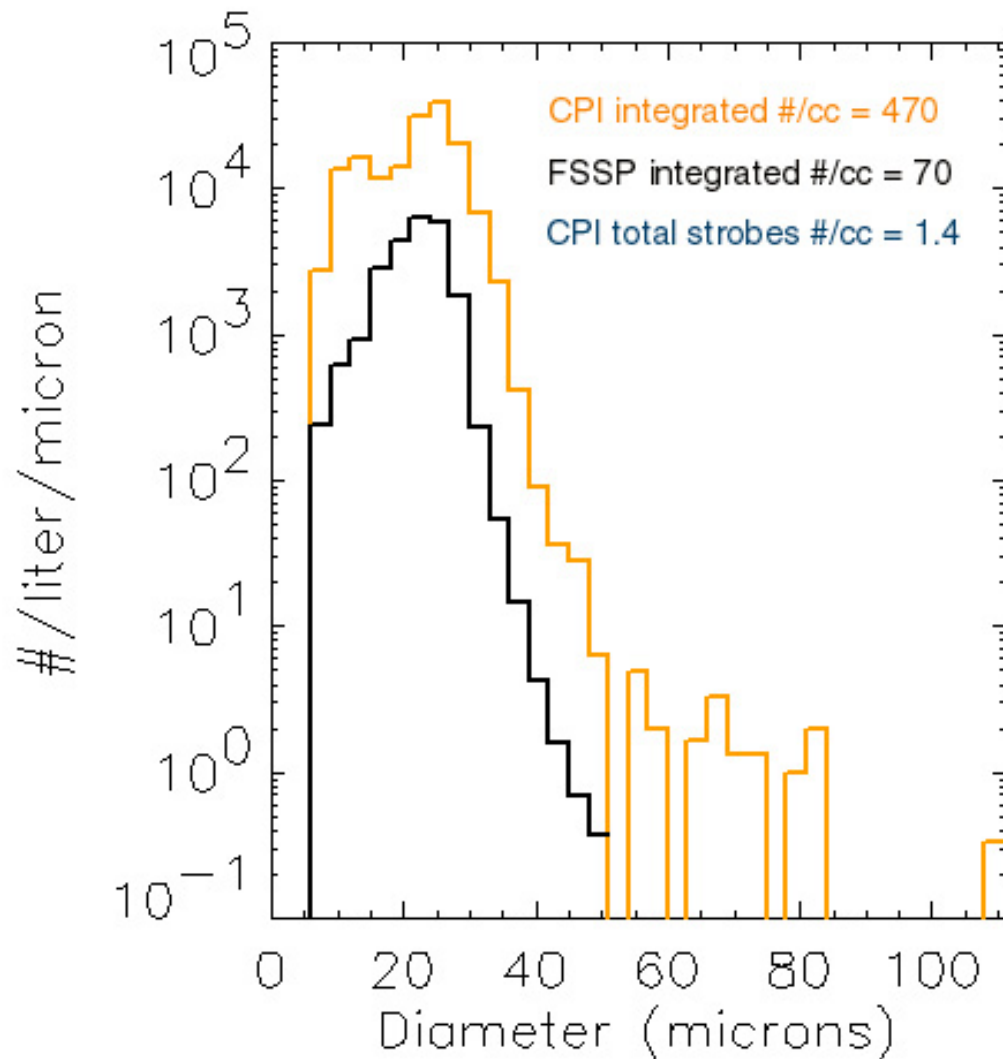


Figure 6: The orange size distribution is the same as the orange one in figure 5 except it has been changed to the physical units $\#/liter/\mu m$. The black size distribution was measured by a FSSP.

The tendency of the CPI to estimate concentrations that are too high can be explained by several factors. Our DOF estimates were a first cut, based on one laboratory run only. The DOF is so small for these small droplets that small errors in the laboratory calibration are likely leading to larger errors in concentration for these small droplets. Errors of this magnitude should not occur for larger particles. A more extensive and accurate laboratory calibration is now warranted. Furthermore, these particle size distributions are based on the imaged particles and the imaged volume (WYSIWYG). The

volume is small so many frames are averaged together to lower statistical errors. The triggering process causes the samples to be conditional instead of random. The regions, such as clear air, where triggering is less likely are under represented in the average. In inhomogeneous cloud this causes the sampling to be biased toward the higher concentration regions. Even in a homogeneous cloud the number of empty frames observed can be below the expected number for random sampling. This is the reason for triggering. With the small sample volume, in low concentration ice clouds nearly all the image frames would otherwise be empty. The wind tunnel was very inhomogeneous. Thus when the PDS thresholds were changed, from a typically used values of 122 – 183 *mV* (200 – 300 in the units of the real time display GUI) to an extremely high value of 610 *mV* (1000), the condition for sampling changed and the effect on the size distribution is noticeable and understandable. At the high setting, the larger drops ($> \sim 100 \mu m$) or high concentration regions of smaller droplets, where coincidence could boost the scattered light signal, were now better able to trigger a flash. This biases the size distribution towards those droplet sizes and towards an overall higher total concentration (X2 in this case) as shown in figure 10. The effects of conditional sampling are decreased at lower PDS thresholds and thus we recommend the lowest settings that rule out false noise triggers for standard operation in field projects. In the above comparisons (figures 7, 8 and 9) we used the more representative spectrum measured at the lower PDS thresholds. Still we must expect biasing due to the conditional sampling, even at low PDS thresholds, in the total concentration measure. It is worth pointing out that this conditional sampling aspect of the CPI is not unique to the instrument. Consider for example the PMS 2D probes. They can go into over load in dense cloud causing the sampling to be non-continuous. Since the amount of overflow caused dead time increases with particle concentration, the lower concentration regions are better represented in the average than the high concentration regions. A final factor must also be considered. The calibration was performed on a particular CPI, the new NSF probe. The data shown in figure 6 was taken with the original NSF probe. The question of variances between probes must still be addressed. The main change between these two probes was that the optical system was folded in order to fit into a smaller package. The CPI used in the wind tunnel belongs to AES and was produced identically to the new NSF probe. Theoretically there are no differences between any of the CPI probes.

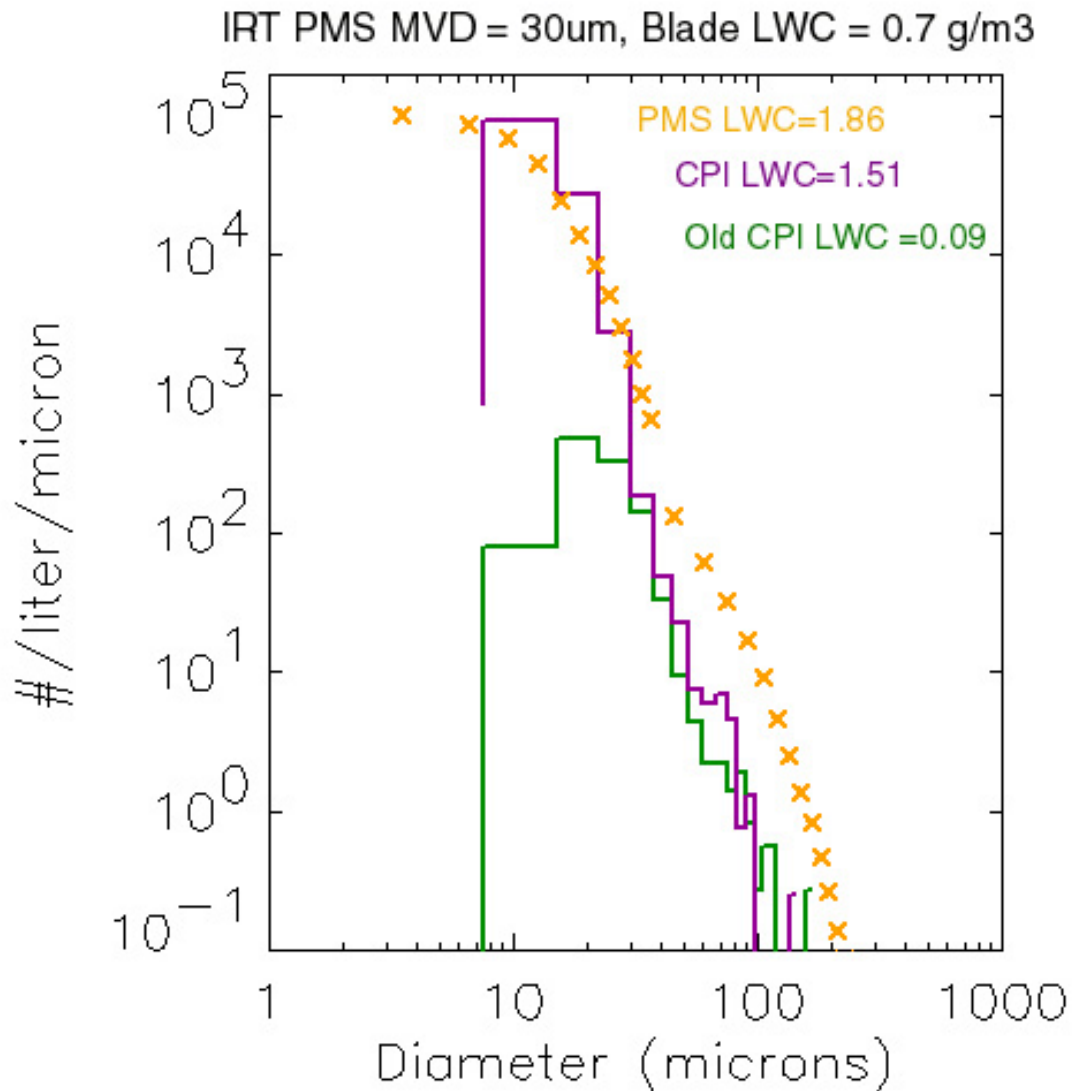


Figure 7: Comparison between the old raw CPI size distribution (green), using D_{app} and a fixed DOF, and the CPI size distribution (purple) using D and variable DOF and the size distribution measured by PMS 1D and FSSP probes (orange) in the NASA icing research wind tunnel. The median volume diameter as measured by the PMS probes was 30 μ m and the liquid water content as measured by an icing blade was 0.7 g/m³.

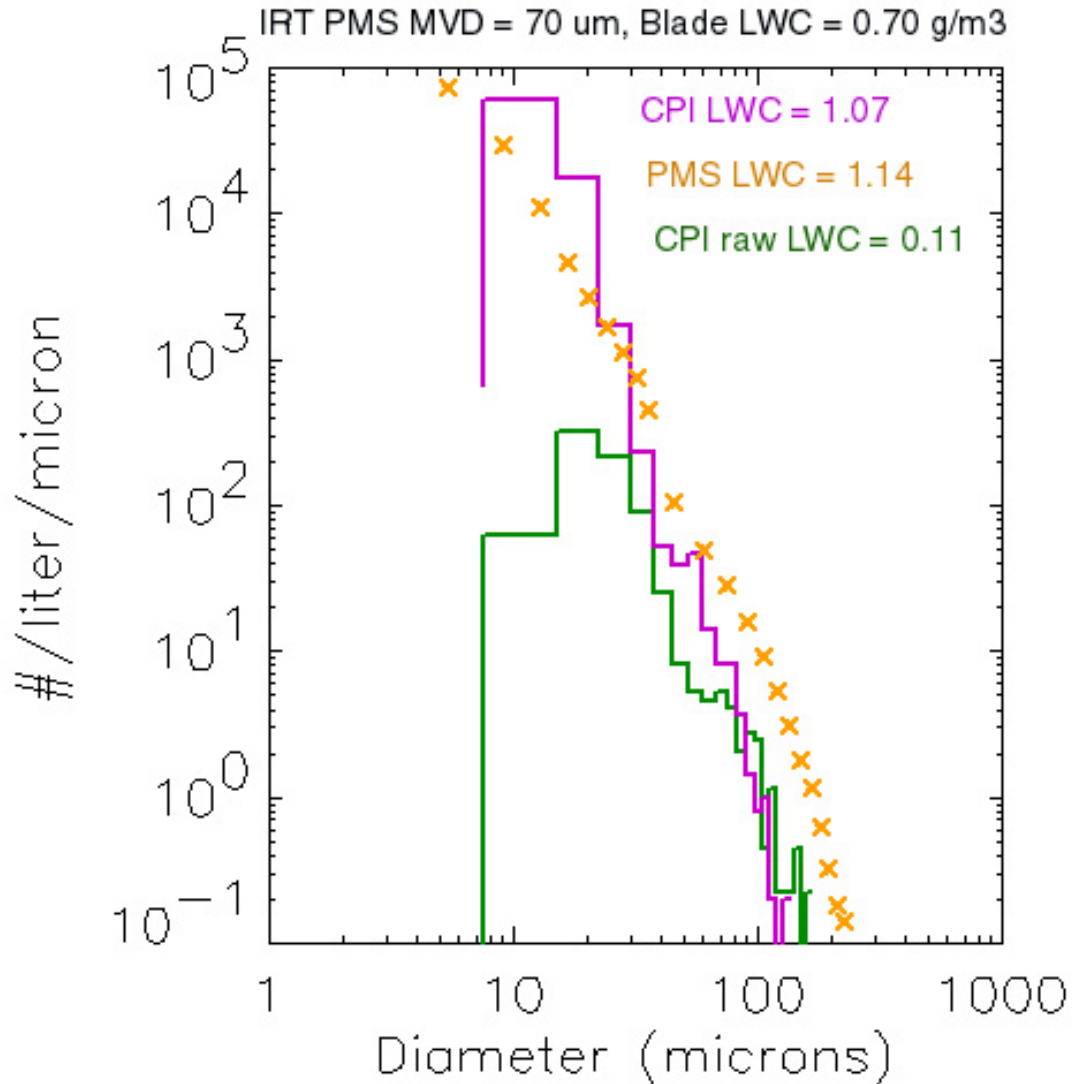


Figure 8: Comparison between the old raw CPI size distribution (green), using D_{app} and a fixed DOF, and the CPI size distribution (purple) using D and variable DOF and the size distribution measured by PMS 1D and FSSP probes (orange) in the NASA icing research wind tunnel. The median volume diameter as measured by the PMS probes was $70 \mu\text{m}$ and the liquid water content as measured by an icing blade was $0.7 \text{ g}/\text{m}^3$.

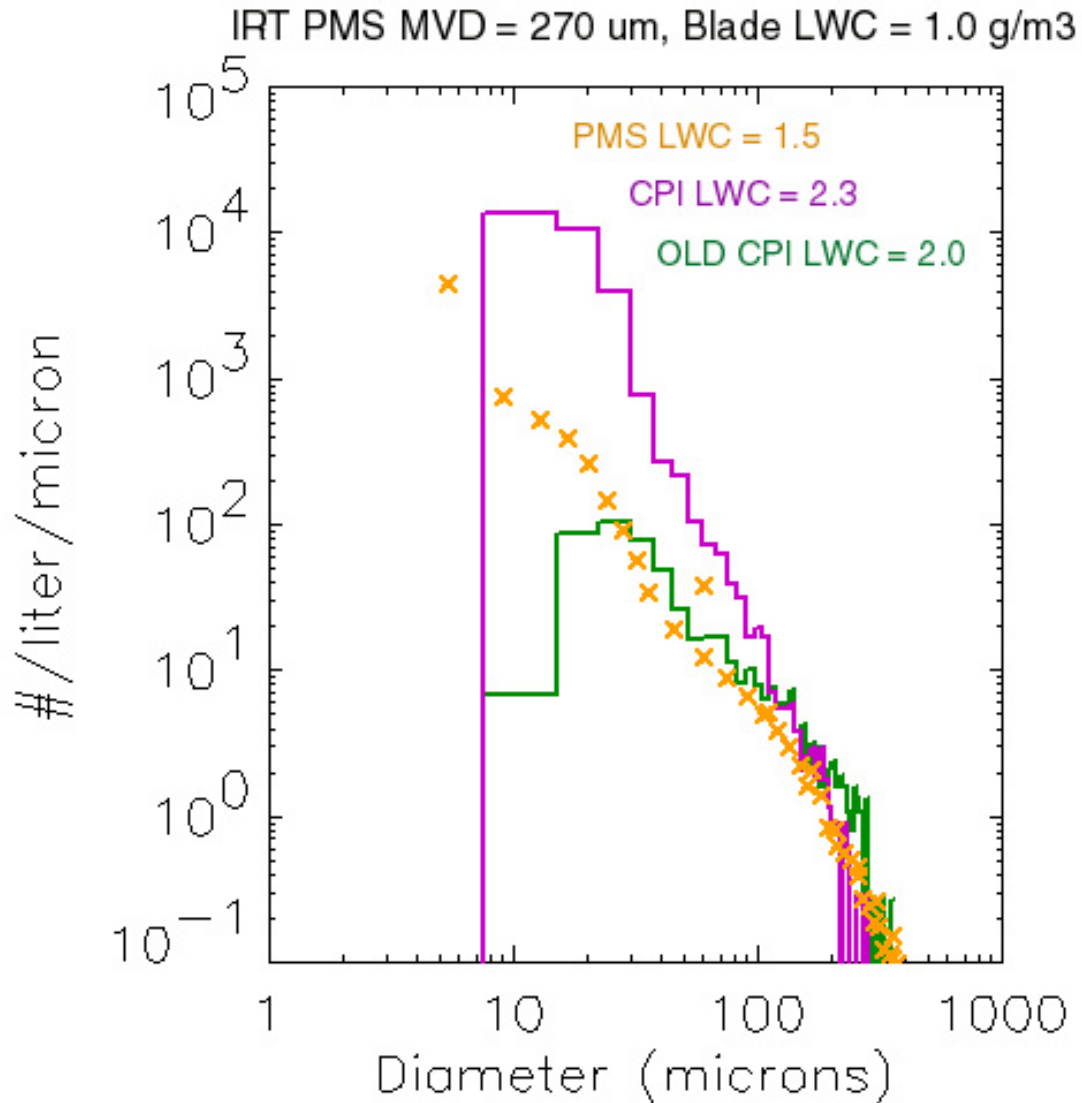


Figure 9: Comparison between the old raw CPI size distribution (green), using D_{app} and a fixed DOF, and the CPI size distribution (purple) using D and variable DOF and the size distribution measured by PMS 1D and FSSP probes (orange) in the NASA icing research wind tunnel. The median volume diameter as measured by the PMS probes was $270 \mu\text{m}$ and the liquid water content as measured by an icing blade was $1.0 \text{g}/\text{m}^3$.

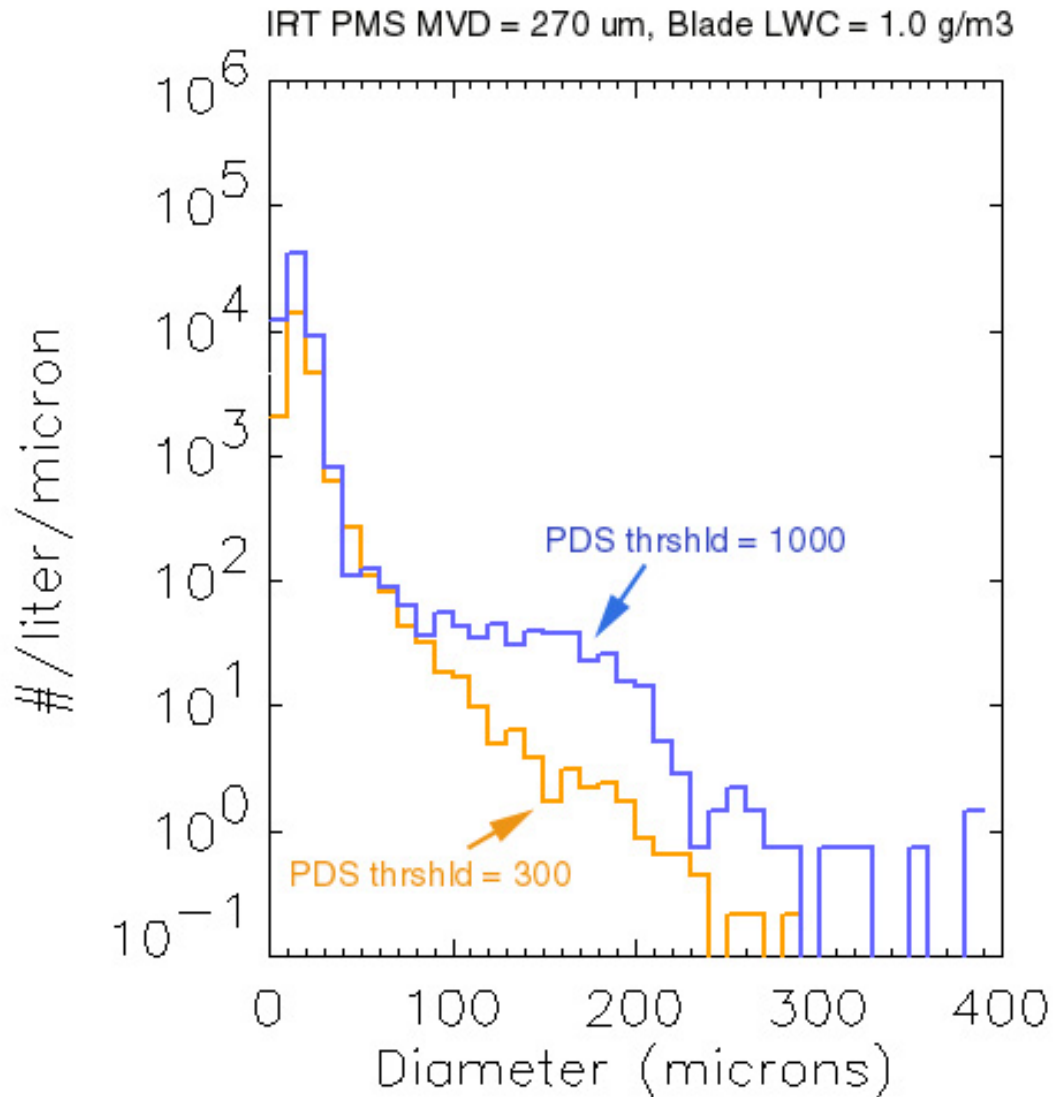


Figure 10: For the wind tunnel conditions of figure 9, we compare the particle size distributions measured by the CPI for two extreme different settings of the PDS thresholds.

Some PDS Data Points

This work has now also established a couple calibration data points for the CPI's particle detection system (PDS). The PDS triggers the imaging laser to flash when both PDS beams are interrupted. The total number of these events in a given time period yields the CPI's total strobes concentration measurement, a measurement similar to

the FSSP concentration. The sensitivity of the PDS to various sized particles for a given threshold setting is not yet very well known. Laboratory studies must be done in order to address this issue. Until then however an occasional data point can be gathered using the real data. This is one example. On figure 6 we see that the total strobes concentration from the CPI is more than an order of magnitude lower than the FSSP concentration. This demonstrates the relative insensitivity of the PDS to these small droplets at the laser power and PDS threshold settings used at that time. These settings are user settable during real time operation and were set at 30.3mW and 183mV respectively for the data shown. It is possible for the total-strobes concentration to be too low due to coincidence effects. Examination of the recorded particle transit times and the fact that the total-strobes concentration correlated very well with the various LWC probes rules out this possibility here. However because the CPI was operated with a long transit time necessary for triggering the imaging laser and no minimum transit time necessary to count strobes, the total strobes concentration was most likely effected by coincidence overcounting.

Discussion and Future Work

This work was a first cut at using diffraction theory and laboratory calibration to improve our estimates of the particle size distributions from the CPI. The sizing and overall shape of the distributions now look very good while sample volume estimates appear too low as the overall concentration appears too high. This is likely due in part to inaccuracies in the laboratory calibration and in part due to conditional sampling. The former will be addressed by a more thorough processing of a more extensive laboratory data set including different sized particles. The later might be addressable by modifying the triggering criteria and accounting for conditional sampling in the algorithms that calculate concentration. We must also do further laboratory studies to understand how to deal with non-spherical particles. We must perform such studies on a number of different CPIs in order to assess whether there are significant differences between them.

Addendum

In order to assess the effectiveness, and applicability to other CPIs, of the algorithm based on the bead data taken using the NSF probe, we applied the correction algorithm to the bead data itself. Data from many different positions in the sample tube were used. A snapshot of part of the slide used in this study using the NSF CPI is shown in figure I. A similar slide was prepared and used with NASA's CPI. A snapshot of part of that slide is shown in figure II. In both cases beads are clumped up in places and there are some objects on the slide smaller than the 32 μm beads. The majority of clumps are easily removed from the data set by the same automated processing that we use for water versus ice discrimination. The small spherical objects are not removed from the data set but are relatively few in number. Thus the majority of objects in the data set are single beads at different positions in the sample tube. The CPI automated processing was used to find their sizes and the algorithm based on the data taken with the NSF probe was applied. The result for the NSF probe bead data is shown in figure III. We see the size distribution is narrowed and shifted to smaller sizes. This is the desired result. There is still considerable error on the side of overestimating the sizes, but it is much better than the raw sizes. Further improvement would likely be obtained by implementing a neural net that uses intensity cross sections as well as the focus values but it is not clear the benefit would be worth the extra complexity. The results for the NASA probe are shown in figure IV. It is very similar to the NSF probe results except the raw spectrum is already narrower than for the NSF data and no further narrowing is achieved by the correction algorithm. It appears the algorithm is equally applicable to both probes.

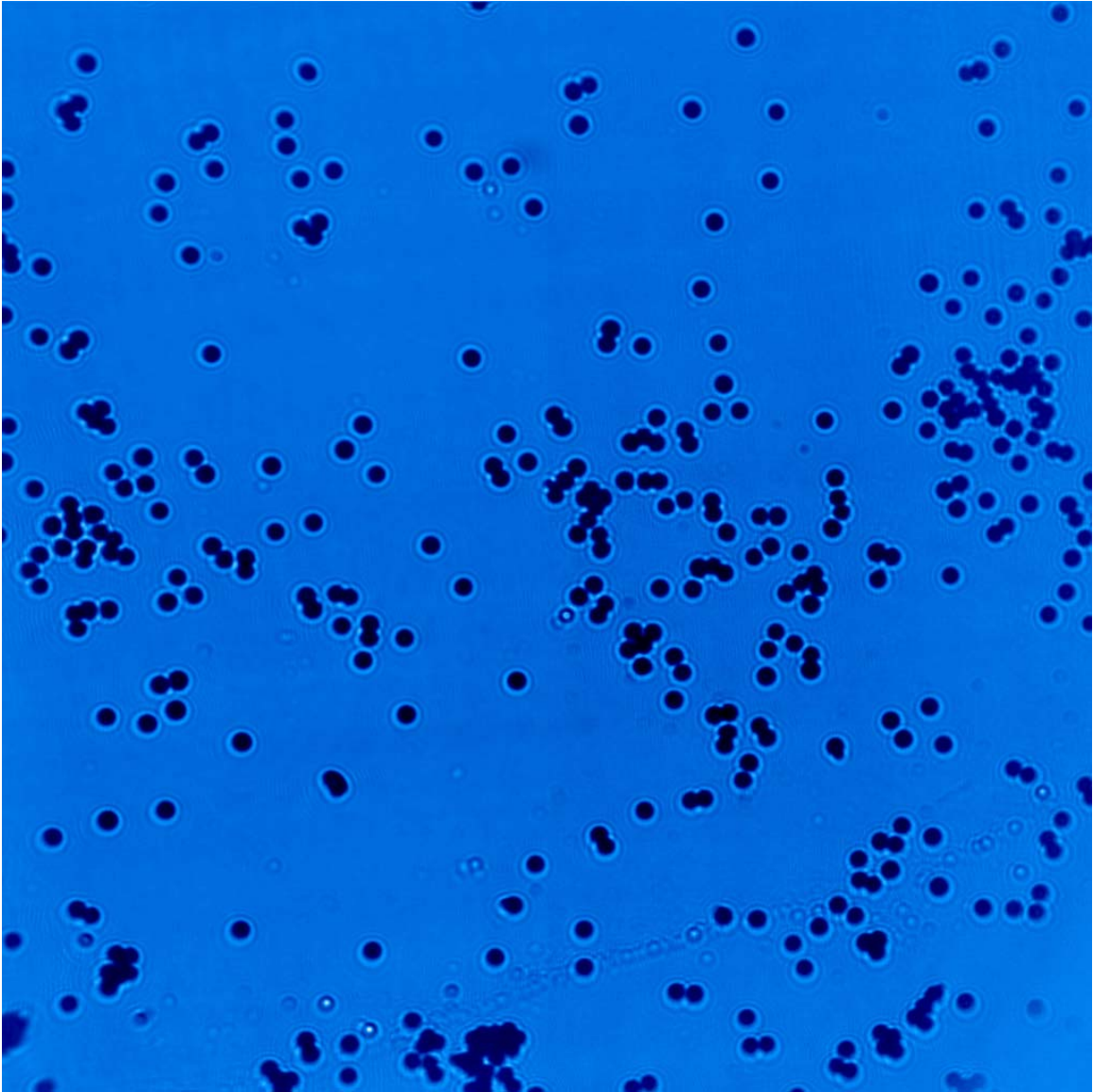


Figure I: One example of a frame of bead data taken in the lab using the NSF CPI.

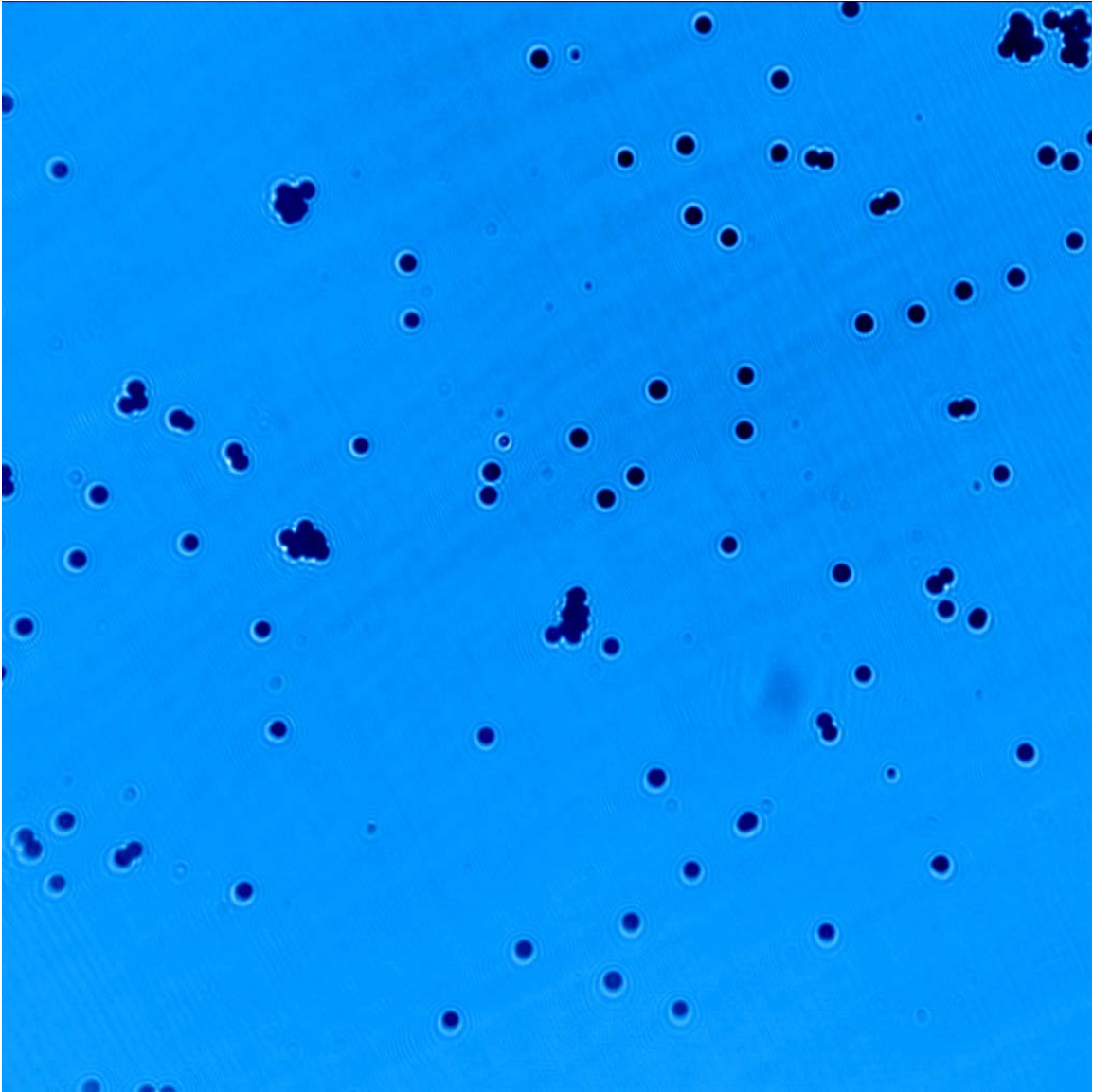


Figure II: One example of a frame of bead data taken in the lab using the NASA CPI.

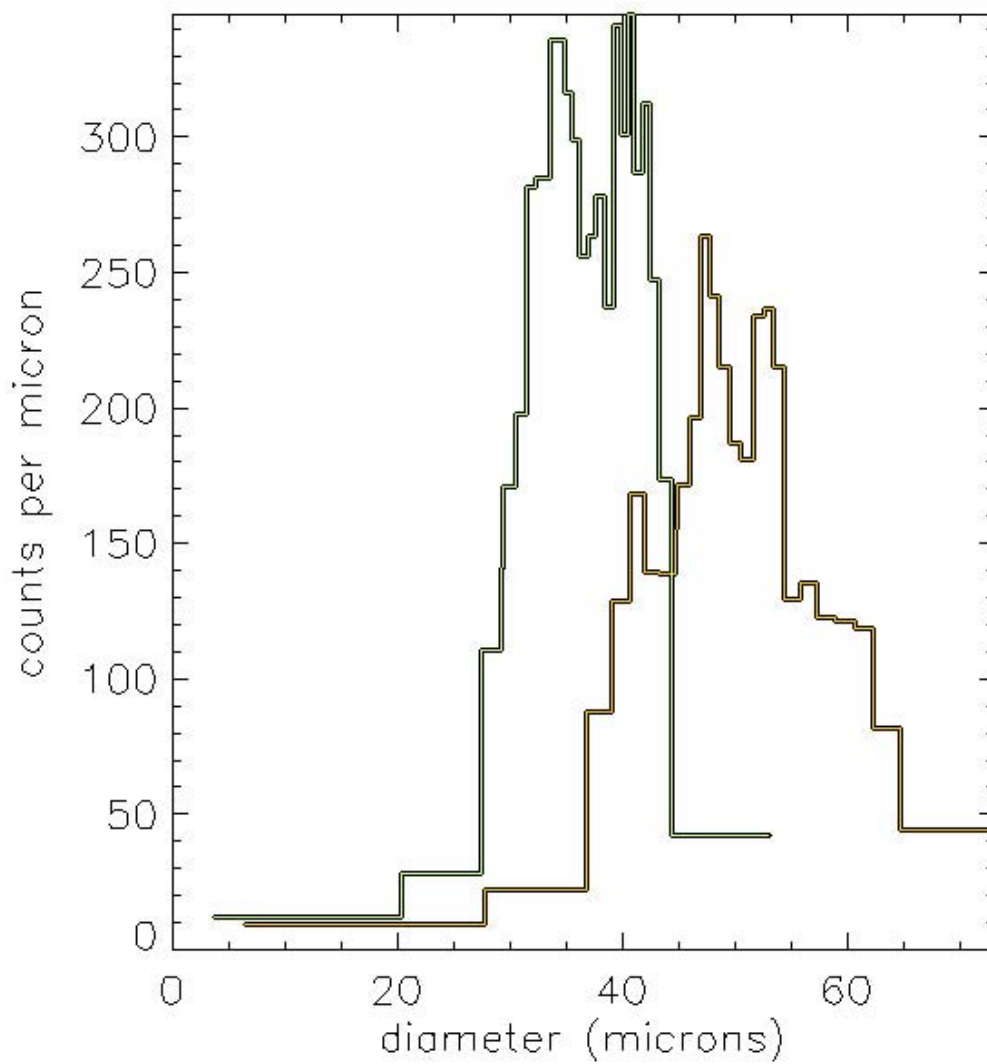


Figure III: NSF CPI bead size distributions before (orange) and after (green) size corrections. Each bin contains 400 beads.

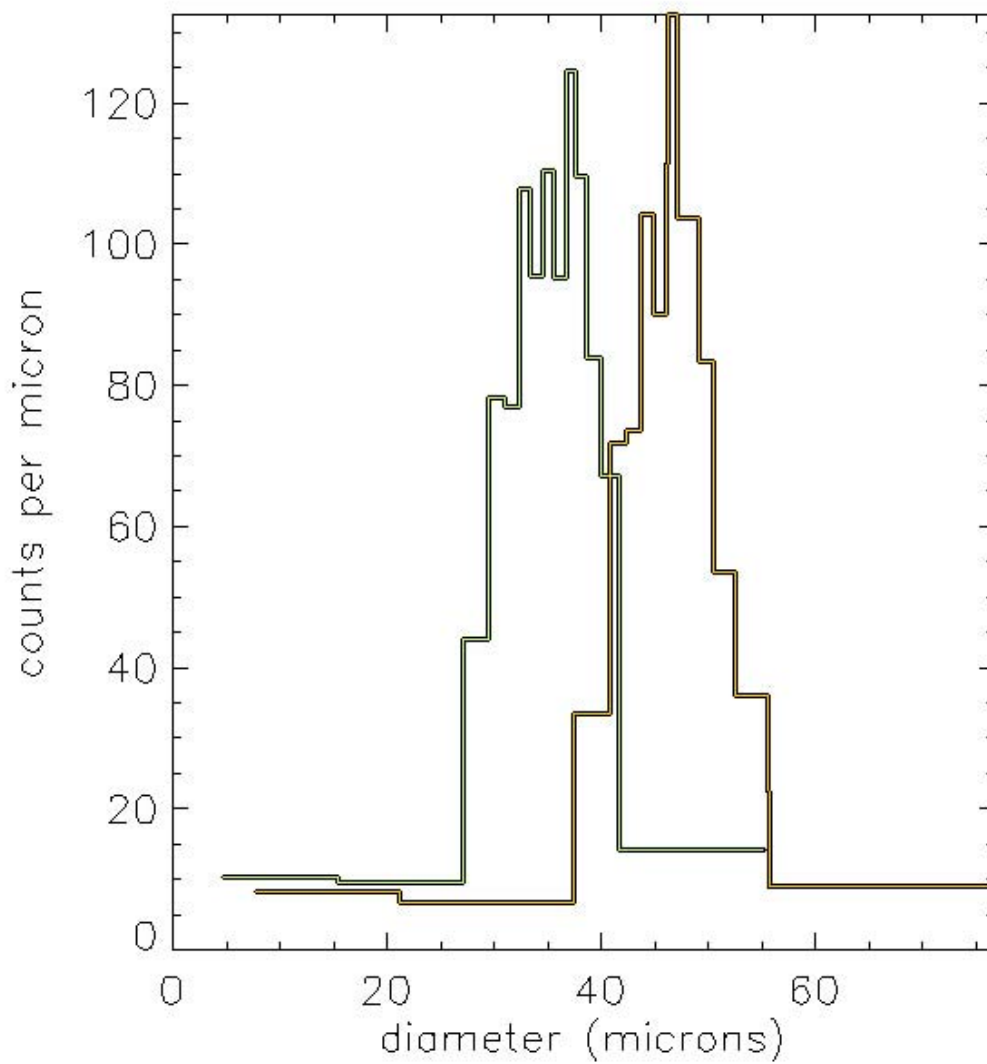


Figure IV: NASA CPI bead size distributions before (orange) and after (green) size corrections. Each bin contains 110 beads.